




# The Time and Energy Dependence of the Vela Pulsar's Pulse Profile in $\gamma$ -Ray

Lin-Li Yan<sup>1,2,3</sup>, Ming-Yu Ge<sup>4</sup>, You-Li Tuo<sup>4</sup> , Ling-jun Wang<sup>4</sup>, and Qing-yong Zhou<sup>5</sup>

<sup>1</sup> School of Mathematics and Physics, Anhui Jianzhu University, Hefei, Anhui 230601, China; [yan.linli@foxmail.com](mailto:yan.linli@foxmail.com)

<sup>2</sup> Key Laboratory of Architectural Acoustics Environment of Anhui High Education Institutes, Hefei, Anhui 230601, China

<sup>3</sup> Key Laboratory of Advanced Electronic Materials and Devices, Anhui Jianzhu University, Hefei, Anhui 230601, China

<sup>4</sup> Key Laboratory of Particle Astrophysics, Institute of High Energy Physics, Chinese Academy of Sciences, Beijing 100049, China

<sup>5</sup> State Key Laboratory of Geographic Information Engineering, Xi'an Institute of Surveying and Mapping, Xi'an 710054, China

Received 2022 January 17; revised 2022 February 10; accepted 2022 February 14; published 2022 March 17

## Abstract

We analyze the time and energy dependence of the Vela pulsar's pulse profile using 13 yr observations from the Large Area Telescope on the Fermi Gamma-ray Space Telescope. It is found that the pulse profile of the Vela pulsar in  $\gamma$ -ray changes with time. We parameterize the pulse profile and find that different shape parameters show fluctuations rather than gradual changes with time. However, these time variation trends are insignificant due to limited statistics. The pulse profile of the Vela pulsar displays clear energy dependence in  $\gamma$ -ray. Different shape parameters are accurately obtained or updated, especially the phase separations among different pulses. Their energy evolution trends are quantified for the first time, which will provide restrictions on current  $\gamma$ -ray emission models. For the Vela pulsar, we also find a turning point at phase. Before and after this phase, the relative intensity of the pulse profile evolves with energy with the opposite trend.

**Key words:** stars: neutron – (stars:) pulsars: individual (Vela) – gamma-rays: stars – Pulsars (1306) – Gamma-ray sources (633)

## 1. Introduction

The Vela pulsar (PSR B0833-45) is one of the strongest  $\gamma$ -ray pulsars in the sky. It has a period of about 89 ms, a spin down rate of  $\dot{P} = 1.25 \times 10^{-13} \text{ s s}^{-1}$  and an energy loss power of  $\dot{E} = 7 \times 10^{36} \text{ erg s}^{-1}$ . It is one of the closest pulsars to the Earth at a distance of  $d = 287 \text{ pc}$  (Dodson et al. 2003). The Vela pulsar has been comprehensively studied over almost all wavelengths from radio, optical, ultraviolet, and X-ray to  $\gamma$ -rays (Gouiffes 1998; Harding et al. 2002; Romani et al. 2005; Manzali et al. 2007; Abdo et al. 2010). These studies indicate that the exact pulse morphology of the Vela pulsar varies as a function of photon energy. From optical to hard X-ray, its pulse profile exhibits a multi-peaked structure, while in radio and  $\gamma$ -ray it is much simpler. In radio band, the pulse profile only has one single pulse, and in  $\gamma$ -ray it consists of two relatively narrow pulses (P1 and P2) with a separation of about 0.42 in phase and a low level “bridge” emission which is usually denoted as P3 (Abdo et al. 2010). In  $\gamma$ -ray, as energy increases, the intensity ratio of P2 to P1 decreases and the intensity of P3 increases.

Many models have been proposed to explore the high-energy  $\gamma$ -ray emission mechanism in the Vela pulsar. In traditional models, the acceleration and emission zones are different but all are inside the light cylinder, such as the polar cap model (Daugherty & Harding 1994), the outer gap model (Cheng et al. 1986a, 1986b, 2000), the slot gap model (Dyks & Rudak 2003) and the annular gap model (Du et al. 2011). For some recent

global magnetospheric models such as the force-free inside and dissipative outside (FIDO) model (Brambilla et al. 2015), the current sheet models (Bai & Spitkovsky 2010; Contopoulos & Kalapotharakos 2010), and the kinetic/particle-in-cell simulations (Cerutti et al. 2016; Philippov & Spitkovsky 2018). They postulate that the high-energy emission originates outside the light cylinder. Almost all these studies focus on modeling the pulse profile of the Vela pulsar to test their models. In Du et al. (2011), the pulse profile of the Vela pulsar in  $\gamma$ -ray could be modeled well by using a three-dimensional magnetospheric model, where P1 and P2 are generated in the annular gap region while P3 is from the core gap. The shape differences of the profile in different energy bands depend on the emission altitude. A two-layer outer gap model in Wang et al. (2011) also compared their modeling pulse profile with Fermi observations, which reveals the existence of P3 between two main pulses, and the energy-dependent movement of P3 is from the azimuthal structure of the outer gap. In this model, the phases of P1 and P2 are determined by the magnetic field structure rather than the energy band. A slot gap which reaches up to two light cylinder radii gives a prediction that the morphology of the pulse profile is related to the radius of curvature of magnetic field lines (Venter et al. 2018), and the modeling results for the pulse profile in a FIDO model also confirm this (Yang & Cao 2021). However, these current simulations do not give a judgment on the change trend of the separation of P1 and P2 for the Vela pulsar's pulse profile, and

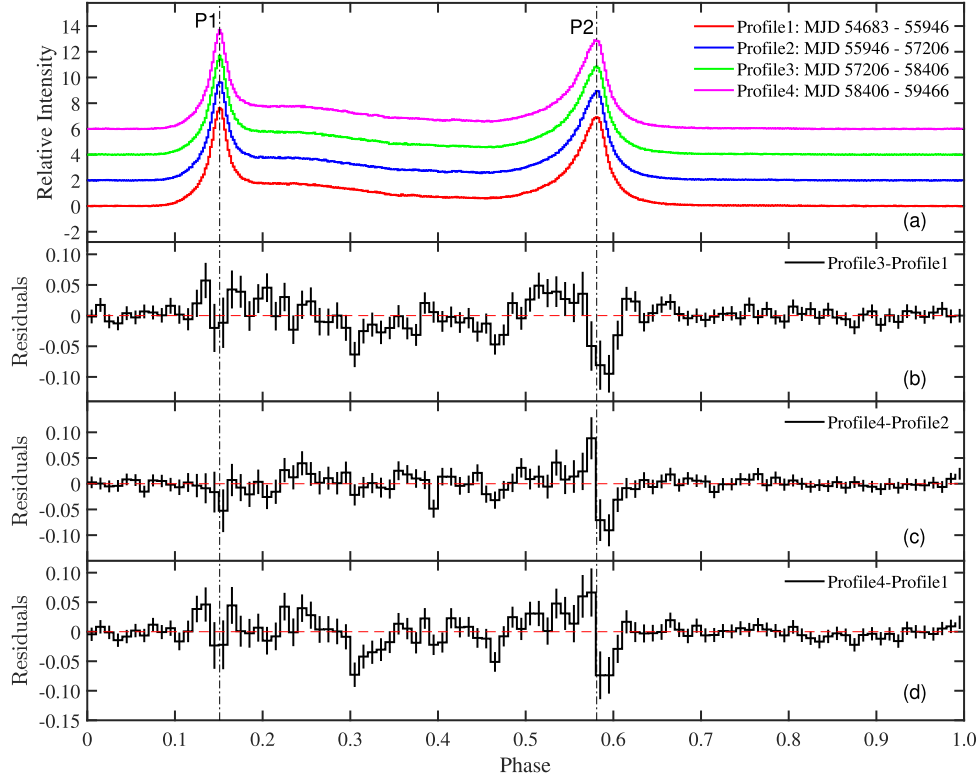


**Figure 1.** The  $\gamma$ -ray profiles of the Vela pulsar in 0.03–300 GeV in different time periods and their difference curves. Every profile in panel (a) is subtracted by its off-pulse count rate and then divided by the mean photon count rate in the whole period. The off-pulse region in phase 0.8–1.0 is selected as background. In order to show them clearly, profiles 2, 3 and 4 are shifted upward by 2, 4 and 6, respectively. Panels (b), (c) and (d): difference curves between profiles in different time periods. The red lines with a constant intensity of 0 are plotted in order to show the change trend of the difference curves. The two vertical lines mark the peak positions of the two pulses.

they only compared modeling pulse shape with observations qualitatively due to the lack of quantitative energy evolution results. All these models are constructed to give time-stable emissions and lack considering the time dependence of the pulse profile. As we know, the shape of a pulse profile of the Vela pulsar is changing with time in the radio band (Palfreyman et al. 2016), but its time-dependence in the  $\gamma$ -ray band has not been studied. Because of the limits of statistics, the quantitative energy evolution of the Vela pulsar’s pulse profile is not given in Abdo et al. (2010).

Since various models make predictions concerning the shape of the pulse profile, better measurement of the pulsed emission will help to explore the radiation properties and physical conditions on the Vela pulsar, and may provide the key to distinguishing different models. The Fermi-Large Area Telescope (LAT) has now collected data since 2008 August 4, gathering 13 yr of observations, and we are able to study the time and energy behaviors of the Vela pulsar’s pulse profile in detail in  $\gamma$ -ray. In this paper, we give an analysis of pulse morphology for the Vela pulsar using Fermi-LAT observations with significantly improved statistics. The new results would

provide further constraints on current models of pulsar’s  $\gamma$ -ray emission. The organization of this paper is as follows: data processing and reduction are presented in Section 2, analysis methods and results are described in Section 3, and discussions on the physical implications of our results are provided in Section 4. Throughout the paper, errors of the parameters are at the one standard deviation level.

## 2. Observations and Data Reductions

The Fermi Gamma-ray Space Telescope is an international and multi-agency space mission that studies the cosmos in the energy range 10 keV–300 GeV. It has two main instruments: the LAT and the Gamma-ray Burst Monitor. The purpose of LAT is to detect  $\gamma$ -rays in the energy range from 20 MeV to 300 GeV, with an effective area of about 8000 cm<sup>2</sup>. It consists of a high-resolution converter tracker, a CsI(Tl) crystal calorimeter and an anti-coincidence detector, which can measure the direction and energy of the  $\gamma$ -rays, and at the same time discriminate the particle background events (Atwood et al. 2009).

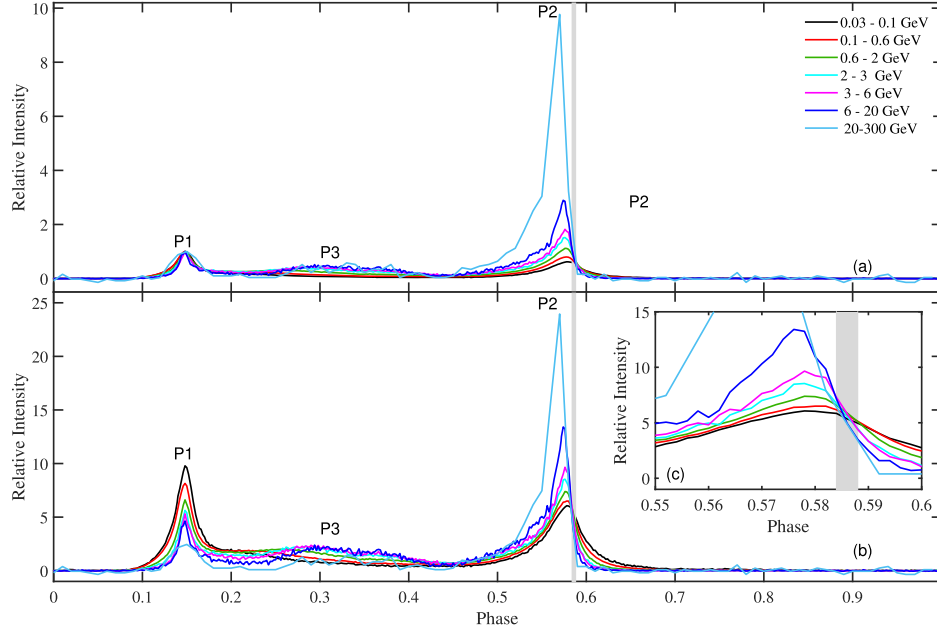


**Figure 2.** The  $\gamma$ -ray profiles of the Vela pulsar in different energy bands. In panel (a), profiles are normalized by the peak intensity of P1 with the off-pulse emission subtracted; In panel (b), profiles are normalized by the mean count rates of each phase bin with the off-pulse emission subtracted. The inset (c) shows the partial enlargement of profiles in phase 0.55–0.60 in panel (b). The gray bar (phase 0.584–0.588) marks the turnover phase interval of pulse intensity change.

The LAT data analysis is accomplished by using the Fermi Science Tools (v11r5p3). First, we use the commands *gtselect* and *gtmktime* to select the events in good time intervals. Then, in order to reduce the contamination from neighboring sources and get pulse profiles with good signal to noise ratio over a broad energy range, photon events in the region of  $\theta < \text{Max}[1.6 - 3\text{Log}_{10}(E_{\text{GeV}}), 1.3]$  deg of the pulsar position are selected (Abdo et al. 2009). The selected photon events are corrected to the solar system barycenter (SSB) and then used to fold pulse profiles in different time epochs and energy bands using the command *gbary* with the solar system ephemerides DE405 and the pulsar position of R.A. = 128°836, decl. = −45°1764 (J2000). The  $\gamma$ -ray events from Modified Julian Date (MJD) 54,683–59,466 (UTC 2008 August 05–2021 September 09) in 0.03–300 GeV are analyzed in this paper.

### 3. Data Analysis

#### 3.1. Timing Analysis

When folding the pulse profile of the Vela pulsar, a long time timing model is needed. We perform a segmented timing analysis for the Vela pulsar. The 13 yr observations of Fermi-LAT in MJD 54,683–59,466 are divided into 85 epochs, and each epoch is approximately 40–60 days. We search for a best spin frequency and use it to fold the pulse profile using events in one day, and a series of pulse times-of-arrival (TOAs) would be obtained in every epoch, then the rotation frequencies and their derivatives could be calculated using these TOAs in

different epochs by the software TEMPO2 (Hobbs et al. 2006). The detailed timing procedure can be found in Ge et al. (2019).

The timing analysis of the Vela pulsar in MJD 54,683–58,826 was performed in detail by Gügercinoğlu et al. (2020), and the analysis in MJD 58,826–59,466 is added by this work. The 85-segment timing model is used to fold the pulse profile in different epochs and energy bands.

#### 3.2. Shape Parameters of Pulse Profile

The integrated pulse profiles in 0.03–300 GeV in different epochs all have two obvious pulses. As shown in Figure 1, the higher pulse at phase 0.15 is denoted as P1, and the other significant pulse at phase 0.58 is signified as P2. When examining the shape of pulse profiles in different energy bands, another pulse between P1 and P2 becomes notable, whose intensity increases as energy increases, and it is denoted as P3, as depicted in Figure 2. To compare these profiles in different energy bands clearly, all the original profiles are normalized by subtracting the mean count rate of the off-pulse region (phase 0.8–1.0) (Grondin et al. 2013) and then divided by the background-subtracted peak intensity of P1. With this normalization method, the peak count rate of P1 is fixed at 1, as displayed in Figure 2(a). The other normalization method is also applied in this work: each profile is subtracted by its off-pulse count rate and then divided by the mean photon count rate in the whole period. The profiles normalized by the second method make it easy to observe the overall energy evolution

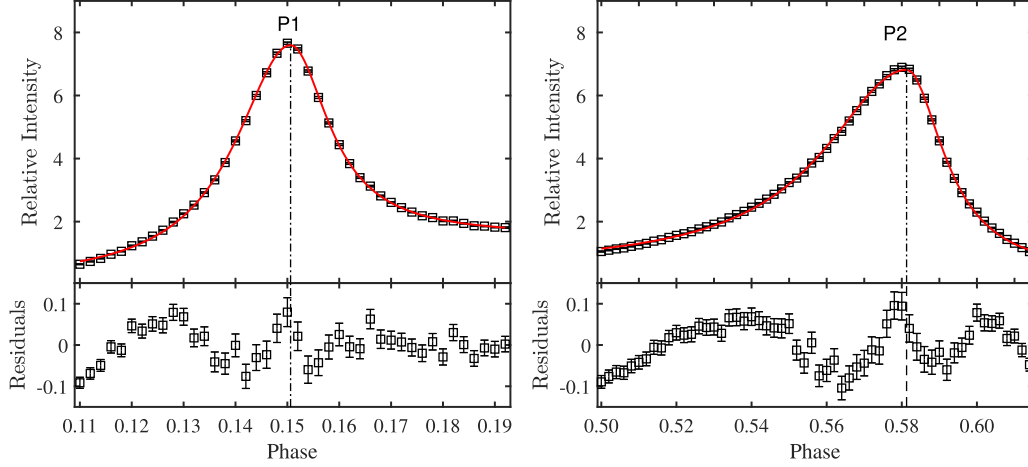


**Figure 3.** The fitting results and residuals of two pulses when using an asymmetric Lorentzian function in Abdo et al. (2010). The pulse profile is in MJD 54,683–59,466 in energy range 0.03–300 GeV, i.e., the sum of profiles 1, 2, 3 and 4 in Figure 1 with background subtracted and normalization. The two vertical lines mark the peak positions of the two pulses which are obtained from the fitting results, and red lines are the fitting curves for two pulses.

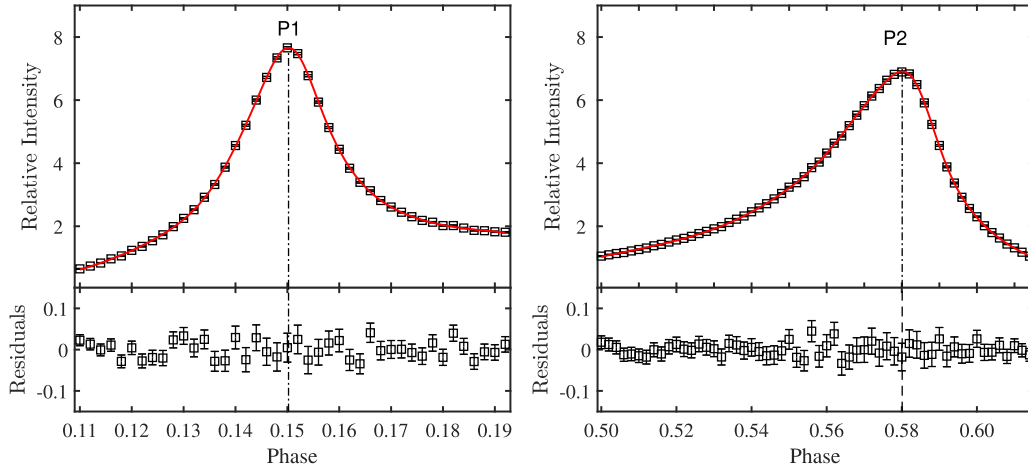


**Figure 4.** The fitting results and residuals of two pulses when using the Gauss4 function. The pulse profile is in MJD 54,683–59,466 in energy range 0.03–300 GeV, i.e., the sum of profiles 1, 2, 3 and 4 in Figure 1 with background subtracted and normalization. The two vertical lines mark the peak positions of the two pulses which are obtained from the fitting results, and red lines are the fitting curves for two pulses.

trend. All the profiles in different epochs or energy bands are normalized by utilizing the second normalization method before fitting them.

In order to investigate the time and energy dependence of a pulse profile in a quantitative way, it is necessary to fit profiles using a suitable function. In Abdo et al. (2010), they relied on an asymmetric Lorentzian function to fit the Vela pulsar's pulse profile. We find that this Lorentzian function cannot describe the shape of a high-precision pulse profile well, especially around peaks P1 and P2, as displayed in Figure 3. We start to build the fitting function for P1 and P2 from two Gaussian functions and increase the number of Gaussian functions to make the fitting residuals uniformly distributed. As shown in Figure 4, we find

that a combination function of four Gaussian functions (denoted as Gauss4) can fit the shape of two pulses well. The fitting residuals are uniformly distributed and their root mean square errors are 0.021 and 0.016 for P1 and P2 respectively when utilizing Gauss4. The uncertainty of intensity for P1 and P2 is comparable to these two root mean square errors, so there is no need to increase the number of Gaussian functions. In the following, we use Gauss4 to fit P1 and P2. As for P3, its shape changes greatly with energy and it is not easy to find a good function to describe it due to the limits of statistics. We only use one Gaussian function to fit P3 to get its peak position.

We use four parameters to characterize the  $\gamma$ -ray pulse profile in different epochs. They are the phase separation

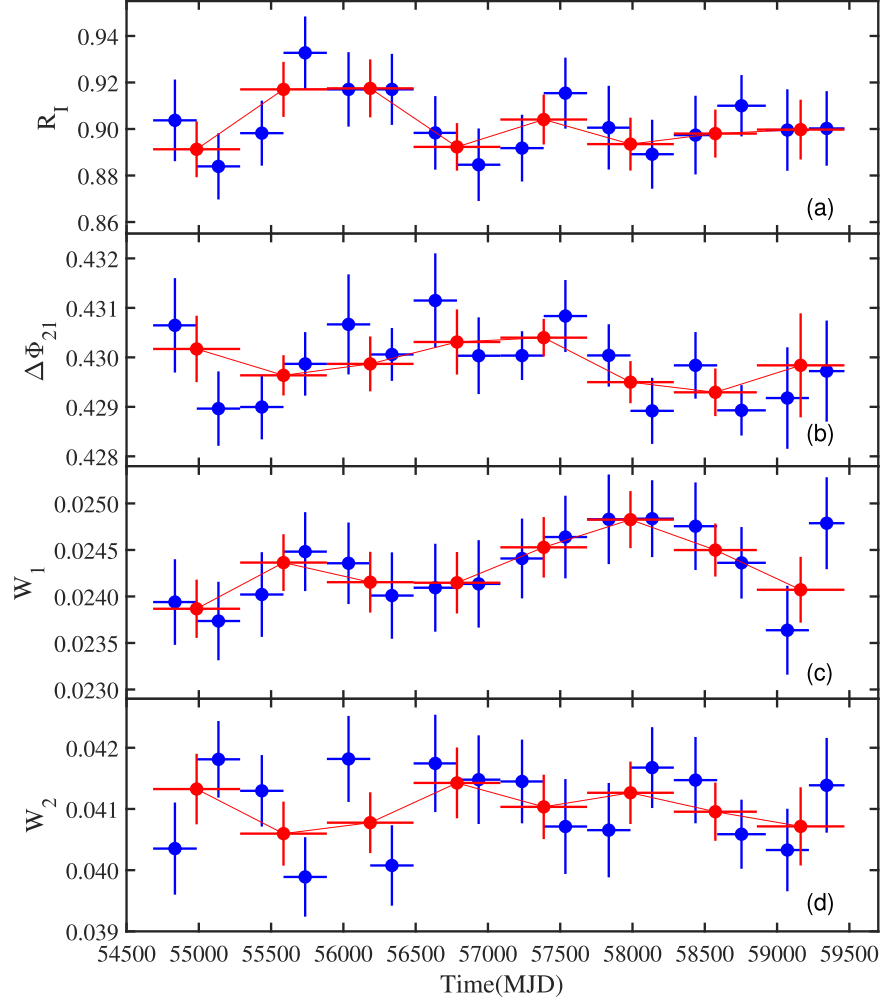


**Figure 5.** The shape parameters of the Vela pulsar’s pulse profile in different periods. The blue data points represent shape parameters of profiles which are over a duration of about 300 days, while the red data points signify parameters of profiles which are over a duration of about 600 days. Panels (a)–(d) feature the peak intensity ratio of P2 to P1 ( $R_I$ ), the phase separation between the two maxima of P1 and P2 ( $\Delta\Phi_{21}$ ), and the FWHMs of P1 and P2 ( $W_1$  and  $W_2$ ), respectively.

between the two maxima of P1 and P2 ( $\Delta\Phi_{21}$ ), peak intensity ratio of P2 to P1 ( $R_I$ ), and full widths at half maximum (FWHMs) of P1 and P2 ( $W_1$  and  $W_2$  respectively) after subtracting the pulse background. When studying the energy evolution of pulse profiles, several additional parameters have been considered. They are the integrated flux ratio within the FWHM of P2 to P1 ( $R_F$ ), the phase separation between the two maxima of P2 and P3 ( $\Delta\Phi_{23}$ ), and the half widths at half maximum (HWHMs) of P1 and P2, which are used to check whether the pulse width changes symmetrically with energy. The left side and right side of P1 are denoted as LP1 and RP1, respectively. The left side and right side of P2 are signified as LP2 and RP2, respectively. We use the same method as that in Ge et al. (2016) to estimate the errors of every shape parameter.

### 3.3. Pulse Profiles in Different Epochs

In this section, the time dependence of the  $\gamma$ -ray profile is studied in two ways: using the profile difference curve and the shape parameters of pulse profile respectively. The profile difference is the difference between two normalized profiles in different epochs, which can exhibit the profile variation directly if the profile changes with time. As shown in Figure 1, the difference curves are not constant in the whole phase. It is clear that the separation between P1 and P2 changes with time, and its change trend is not monotonic.

To explore the time dependence of the shape of the Vela pulsar’s profile in a quantitative manner, all the observations are divided into 16 periods. The integrated pulse profile in every period is over a duration of about 300 days and is fitted by using function Gauss4 (described in Section 3.2). All the

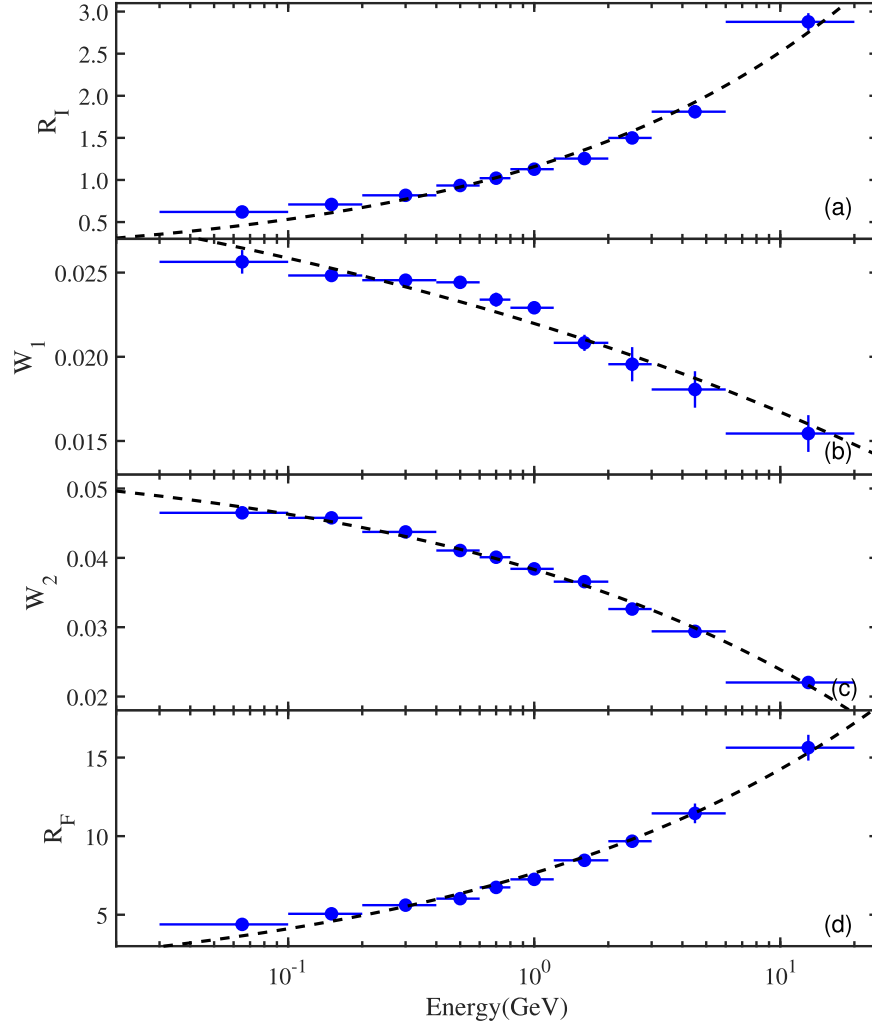


**Figure 6.** The shape parameters of the Vela pulsar's pulse profile in different energy bands. The blue data points in panels (a)–(d) represent the peak intensity ratio of P2 to P1 ( $R_1$ ), the FWHMs of P1 and P2 ( $W_1$  and  $W_2$ ), and the integrated flux ratio within the FWHM of P2 to P1 ( $R_F$ ), respectively. The black dashed lines are the fitting curves for blue data points.

observations are also divided into eight periods (each period has a time span of about 600 days) to explore the long term evolution trend of pulse shape. As affirmed in Figure 5, all the four shape parameters do not show stable evolution trends, but present different fluctuations over time, which are different with the behavior of the Crab pulsar (Ge et al. 2016). We use a reduced  $\chi^2$  ( $\chi_r^2$ , Equation (1)) to evaluate the significance of time variations for different parameters,

$$\chi_r^2 = \frac{1}{N-1} \sum_i \frac{[y_i - \text{mean}(y_i)]^2}{\sigma_i^2}, \quad (1)$$

where  $y_i$  represents a shape parameter in one period,  $\sigma_i$  is the uncertainty of  $y_i$  and  $N$  is the number of periods. All the  $\chi_r^2$  for different shape parameters are lower than 1, so their time

variations are not significant considering the uncertainties of shape parameters.

#### 3.4. Pulse Profiles in Different Energy Bands

In previous studies (Abdo et al. 2009, 2010), it is found that the pulse profile of the Vela pulsar in  $\gamma$ -ray shows a clear energy dependence. With the analysis of 13 yr Fermi-LAT observations, it is convenient to study the energy evolution of the Vela pulsar's pulse profile in detail in this work. As displayed in Figure 2, the overall distribution of  $\gamma$ -ray photons in phase changes with energy (Panel (b)). The intensities of P2 and P3 increase with increasing energy and this trend turns over at phase about 0.586. Before and after phase 0.586, the energy evolution trend of pulse intensity is opposite, i.e., the intensity of the right side of P2 decreases as energy increases.



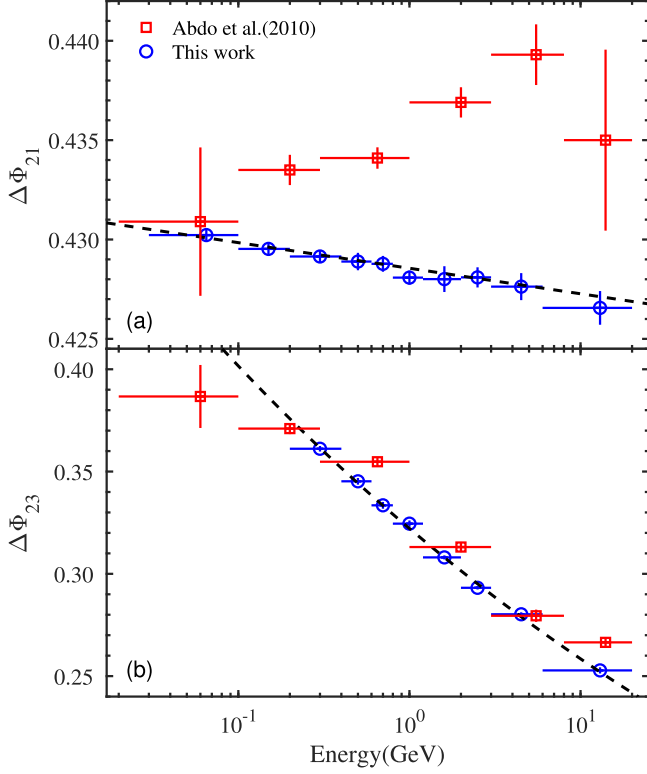


**Figure 7.** The phase separations among three pulses of the Vela pulsar’s pulse profile in different energy bands. The blue circle symbols in panels (a)–(b) are the separations between P2 and P1, and P2 and P3, respectively, and they are obtained in this work. The red square data points are from the results in Abdo et al. (2010).

There is only one turning point at phase for the energy evolution of the pulse profile. The  $\gamma$ -ray photons higher than 20 GeV are only 0.2% over the total photons in 0.03–300 GeV, so we only calculate the shape parameters for the pulse profiles in 0.03–20 GeV.

The quantitative evolution results would be obtained after fitting pulse profiles in different energy bands (Figures 6, 7, 8). Both the peak intensity ratio and flux ratio of P2 to P1 ( $R_b$ ,  $R_f$ ) increase as energy is increasing, while the widths of P1 and P2 ( $W_1$ ,  $W_2$ ), the phase separations between P1 and P2 ( $\Delta\Phi_{21}$ ), and P2 and P3 ( $\Delta\Phi_{23}$ ) display opposite energy evolution trends with  $R_f$ , as depicted in Figures 6 and 7. When energy is larger than 0.7 GeV, the intensity of P2 begins to be stronger than P1, and their ratio is about 3.0 when energy reaches 20 GeV. From 0.03 to 20 GeV, the width of P1 drops by  $\sim 0.01$  while P2 drops by  $\sim 0.025$ , i.e., the width of P2 changes faster than that of P1. The following energy evolution trend fitting results for  $W_1$  and  $W_2$  also confirmed this.

Because of using an unsuitable function when fitting the pulse profile of the Vela pulsar, results in Abdo et al. (2010) are different from ours, especially the separation of P1 and P2 (Figure 7). We only study the parameter  $\Delta\Phi_{23}$  in 0.2–20 GeV

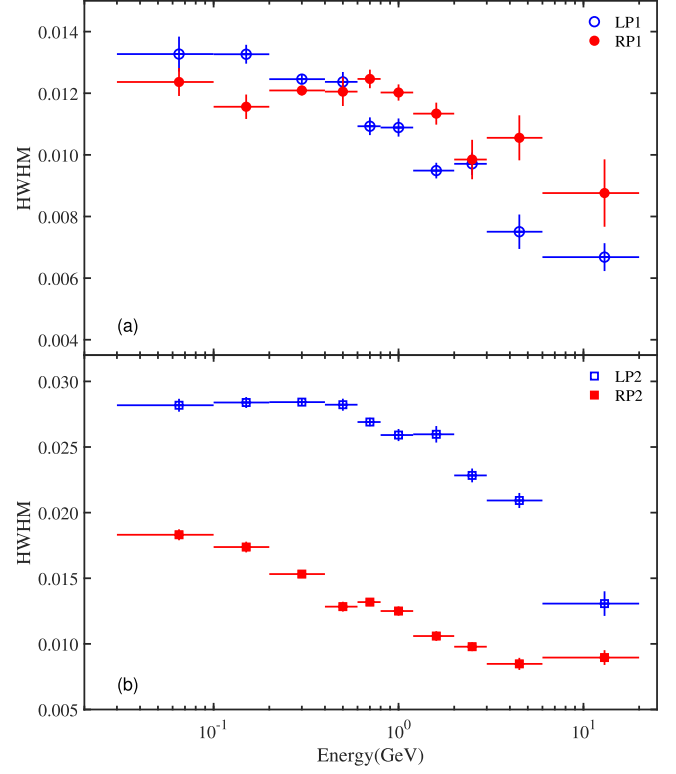


**Figure 8.** The HWHMs of P1 and P2 for the Vela pulsar’s pulse profile in different energy bands. The blue hollow circle symbols in panel (a) represent the HWHM of the left side of P1 (LP1), while the red filled circle symbols signify the HWHM of the right side of P1 (RP1). In panel (b), the blue hollow square symbols correspond to the HWHM of the left side of P2 (LP2), while the red filled square symbols represent the HWHM of the right side of P2 (RP2).

given that P3 becomes clear when energy is higher than 0.2 GeV. The phase separation of P1 and P2 decreases gradually from 0.03 to 20 GeV with a drop of about 0.003, which is very small and hard to detect when using an unsuitable fitting function or with short-time observations. In Abdo et al. (2010), the authors relied on asymmetric Lorentzian functions to fit two pulses. These Lorentzian functions cannot fit the shape around the peak of two pulses well, as shown in Figure 3. The difference between our results and those in Abdo et al. (2010) comes from the choice of fitting function. Although the phase separation of P2 and P3 decreases significantly with increasing energy, the trend is consistent with the results in Abdo et al. (2010). The drop of  $\Delta\Phi_{23}$  in 0.2–20 GeV is about 0.36, which is much larger than  $\Delta\Phi_{21}$ . The phase deviation caused by the selection of the fitting function does not affect the energy evolution trend of  $\Delta\Phi_{23}$ . The symmetry of P1 and P2 is also considered in this work. As displayed in Figure 8, we find that the shape of P1 is almost symmetrical, while the shape of P2 is asymmetric in the whole  $\gamma$ -ray bands. The evolution trend of the left half-width and right half-width of P1 and P2 is basically the same.

**Table 1**  
The Fitting Results of Shape Parameters

$Y$	$c_1$ $\times 10^{-2}$	$c_2$ $\times 10^{-2}$	$c_3$ $\times 10^{-2}$
$R_I$	$115.86 \pm 3.93$	$33.75 \pm 1.88$	0
$W_1$	$-1.48 \pm 1.30$	$13.22 \pm 11.22$	$3.68 \pm 1.27$
$W_2$	$-1.78 \pm 0.31$	$25.76 \pm 3.84$	$5.61 \pm 0.29$
$R_F$	$765.29 \pm 14.59$	$27.02 \pm 1.12$	0
$\Delta\Phi_{21}$	$42.86 \pm 0.01$	$-0.13 \pm 0.01$	0
$\Delta\Phi_{23}$	$32.22 \pm 0.007$	$-9.57 \pm 0.19$	0

In order to quantify the evolutionary trends of pulse shape, we use a power function  $Y = c_1 * E(P\text{keV})^{c_2}$  to fit different shape parameters except for  $W_1$  and  $W_2$ . It is necessary to add an extra constant  $c_3$  to obtain acceptable fitting results for the parameters  $W_1$  and  $W_2$ . Here  $Y$  represents different shape parameters, and  $c_1$ ,  $c_2$ ,  $c_3$  are coefficients of the evolution. The best-fitting parameters of energy evolution trends are listed in Table 1. The fitting results of  $W_1$  have large uncertainties, but the other shape parameters feature clear energy evolution trends.

#### 4. Discussion

In this work, we find that the pulse profile of the Vela pulsar in  $\gamma$ -ray is changing with time, and its change behavior is different from the Crab pulsar. The shape parameters of the Crab pulsar exhibit gradual changes with time both in radio and X-ray bands (Lyne et al. 2013; Ge et al. 2016), while the shape parameters of the pulse profile for the Vela pulsar display fluctuations over time rather than gradual changes (Figure 5), and fluctuations among different shape parameters are not synchronous. However, these time variation trends of shape parameters in  $\gamma$ -ray are insignificant and may just be statistical fluctuations in the data. Collecting more data over a longer period of time may enable the acquisition of exact time variation results for the Vela pulsar's pulse profile in the future.

In the radio band, the pulse profile of the Vela pulsar changes with time by analyzing its pulse width and bright pulse rate (Palfreyman et al. 2016). If the pulse profile in  $\gamma$ -ray also shows a significant time variation trend, the pulse changes with time may arise from the same activity from the Vela pulsar. In X-ray, Durant et al. (2013) studied the jet's shape and found that it has a helical structure. They thought that the free precession of the neutron star may lead to this observation result. If the Vela pulsar is indeed precessing, the long-term timing may be able to detect it and the pulse shape in multi-wavelength would change with time. However, the long-term timing detection is complicated by glitching, and the study on the time dependence of the pulse profile relies on statistics. In this work, the time variation trends for different shape parameters in  $\gamma$ -ray are not significant due to the limit of

statistics. Gathering more observations, it may be easy to find a clear time dependence for the Vela pulsar's pulse profile in the future.

The pulse profile of the Vela pulsar shows clear energy dependence in  $\gamma$ -ray. As energy increases, the intensities of P2 and P3 increase over P1, and the widths of P1 and P2 decrease. All these results are consistent with some previous observational and simulation results (Abdo et al. 2010; Du et al. 2011; Venter et al. 2018; Yang & Cao 2021). The phase separations among three pulses are not determined well in previous studies, but accurate values and evolutionary trends for them are obtained in this work. As shown in Figure 7, the phase separations between P1 and P2, and P2 and P3 decrease as energy increases. The phase separation reflects the relative position of the radiation regions. The energy dependence of phase separations and widths for three pulses may originate from the "stratified" structure of the radiation region (Cheng et al. 1986a, 1986b; Du et al. 2011), i.e., photons of different energies are produced in emission regions with different sizes at different latitudes. Different high energy emission models could predict the general energy evolution trend of pulse shape, and the quantitative evolutionary results (Table 1) will provide restrictions on these models and help to improve them.

For the Vela pulsar, as displayed in Figure 2, we also find a turning point at phase  $\sim 0.586$  where the energy evolution trends of the pulse intensity experience a reversal. At this turning phase, the derivative of spectral index with respect to energy would reach a local minimum (Yan et al. 2022). A detailed research effort on the phase-resolved spectrum is required to verify this in the future.

#### Acknowledgments

We thank the referee for his/her very helpful suggestions and comments. We thank the High Energy Astrophysics Science Archive Research Center for maintaining its online archive service that provided the data used in this research. This work is supported by the National Natural Science Foundation of China (NSFC, Grant Nos. 11903001, U1938109, U1838201, U1838202 and 42004004), the Key Research Foundation of Education Ministry of Anhui Province (KJ2019A0787) and the Doctor Foundation of Anhui Jianzhu University 2019 (2019QDZ14).

#### ORCID iDs

You-Li Tuo  <https://orcid.org/0000-0003-3127-0110>

#### References

- Abdo, A. A., Ackermann, M., Ajello, M., et al. 2010, *ApJ*, **713**, 154
- Abdo, A. A., Ackermann, M., Atwood, W. B., et al. 2009, *ApJ*, **696**, 1084
- Atwood, W. B., Abdo, A. A., Ackermann, M., et al. 2009, *ApJ*, **697**, 1071
- Bai, X.-N., & Spitkovsky, A. 2010, *ApJ*, **715**, 1282
- Brambilla, G., Kalapotharakos, C., Harding, A. K., et al. 2015, *ApJ*, **804**, 84



- Cerutti, B., Philippov, A. A., & Spitkovsky, A. 2016, *MNRAS*, 457, 2401
- Cheng, K. S., Ho, C., & Ruderman, M. 1986a, *ApJ*, 300, 500
- Cheng, K. S., Ho, C., & Ruderman, M. 1986b, *ApJ*, 300, 522
- Cheng, K. S., Ruderman, M., & Zhang, L. 2000, *ApJ*, 537, 964
- Contopoulos, I., & Kalapotharakos, C. 2010, *MNRAS*, 404, 767
- Daugherty, J. K., & Harding, A. K. 1994, *ApJ*, 429, 325
- Dodson, R., Legge, D., Reynolds, J. E., & McCulloch, P. M. 2003, *ApJ*, 596, 1137
- Du, Y. J., Han, J. L., Qiao, G. J., et al. 2011, *ApJ*, 731, 2
- Durant, M., Kargaltsev, O., Pavlov, G. G., et al. 2013, *ApJ*, 763, 72
- Dyks, J., & Rudak, B. 2003, *ApJ*, 598, 1201
- Ge, M. Y., Lu, F. J., Yan, L. L., et al. 2019, *NatAs*, 3, 1122
- Ge, M. Y., Yan, L. L., Lu, F. J., et al. 2016, *ApJ*, 818, 48
- Gouiffès, C. 1998, in *Neutron Stars and Pulsars: Thirty Years after the Discovery*, 363
- Grondin, M.-H., Romani, R. W., Lemoine-Goumard, M., et al. 2013, *ApJ*, 774, 110
- Gügercinoglu, E., Ge, M. Y., Yuan, J. P., et al. 2022, *MNRAS*, 511, 425
- Harding, A. K., Strickman, M. S., Gwinn, C., et al. 2002, *ApJ*, 576, 376
- Hobbs, G. B., Edwards, R. T., & Manchester, R. N. 2006, *MNRAS*, 369, 655
- Lyne, A., Graham-Smith, F., Weltevrede, P., et al. 2013, *Sci*, 342, 598
- Manzali, A., De Luca, A., & Caraveo, P. A. 2007, *ApJ*, 669, 570
- Palfreyman, J. L., Dickey, J. M., Ellingsen, S. P., et al. 2016, *ApJ*, 820, 64
- Philippov, A. A., & Spitkovsky, A. 2018, *ApJ*, 855, 94
- Romani, R. W., Kargaltsev, O., & Pavlov, G. G. 2005, *ApJ*, 627, 383
- Venter, C., Barnard, M., Harding, A. K., et al. 2018, *Pulsar Astrophysics the Next Fifty Years*, 337, 120
- Wang, Y., Takata, J., & Cheng, K. S. 2011, *MNRAS*, 414, 2664
- Yan, L. L., Tuo, Y. L., Ge, M. Y., et al. 2022, *ApJ*, accepted
- Yang, X., & Cao, G. 2021, *ApJ*, 909, 88